Materials Today Bio 32 (2025) 101803

Contents lists available at ScienceDirect

Materials Today Bio

journal homepage: www.journals.elsevier.com/materials-today-bio

Destruction of virus particles via mechanical and chemical virucidal activity of nanocolumnar copper thin films

Keisuke Shigetoh *, Yusuke Hirata, Nobuhiko Muramoto, Nobuhiro Ishida

Toyota Central R&D Labs., Inc., 41-1 Yokomichi, Nagakute, Aichi, 480-1192, Japan

ARTICLE INFO

Keywords:
Antiviral coatings
High-speed atomic force microscopy
Image analysis
Nanostructures
Aerosols
Bacteriophage

ABSTRACT

Human-generated droplets, which facilitate the transmission of viral infections, include large droplets and aerosols. The drying rates of these droplets upon adhesion to a surface vary significantly owing to the wide range of their sizes (~nine orders of magnitude). Consequently, combating viruses requires distinct strategies under wet and dry conditions. However, studies that account for these two contrasting conditions are lacking. In the present study, we replicated these conditions and investigated the topographical properties of enveloped bacteriophages as an indicator of viral integrity *via* high-speed atomic force microscopy. Under wet conditions, a reduction in the virus particle volume was observed only on a nanocolumnar copper (NC-Cu) thin film and not on a chemically stable nanocolumnar cupric oxide (NC-CuO) thin film. In contrast, under dry conditions, virus particles lost their shape integrity on both NC-CuO and NC-Cu films. The deformation of virus particles on the NC-CuO film under dry conditions suggests a mechanism distinct from the chemical activity of Cu (*i.e.*, mechanical activity). These results indicate that dry conditions trigger the mechanical activity of nanostructured surfaces. This highlights the significance of nanostructure-induced mechanical activity in virus inactivation under dry conditions, such as those involving viruses in small droplets or aerosols.

1. Introduction

The pandemic potential of viruses is a threat to human health and the global economy [1,2]. Viruses contained in droplets and aerosols, or even intentionally dried viruses, maintain their infectious activity on surfaces (such as plastics) for several to tens of hours [3–6]. Therefore, transmission *via* contact with solid surfaces and resuspension of pathogen-laden aerosols cannot be ignored [3,4,7]. Immediate inactivation of viruses adhered on solid surfaces is an effective approach to addressing this concern. The formation of nanoscale protrusions on solid surfaces is a potential method to accord surfaces with antiviral activity. This method is aimed at applying the mechanical activity to viruses, given its successful application to bacteria by mimicking the protrusions on the wings of insects, known as the mechano-bactericidal activity [8–10]. Aluminum and silicon with nanostructures on their surfaces can inactivate viruses [11,12]. Transmission electron microscopy (TEM) images of pierced human parainfluenza virus by nanospike silicon [12] have recently afforded clear evidence for mechanical activity. However, the reduction in viral activity due to mechanical activity is less than one order of magnitude for 3 h of contact [11,12], which is lower than that achievable using other well-known antiviral materials that release ions or reactive oxygen species (ROS), such as copper, silver, and their related compounds [13,14].

We previously proposed a nanocolumnar copper (NC-Cu) thin film aimed at utilizing the nanostructure-imparted mechanical activity along with the Cu-imparted chemical activity, which we called mechano-chemo-virucidal activity, against viruses [15]. The fabricated NC-Cu films showed excellent performance wherein the infectious activity of bacteriophages was reduced by five orders of magnitude within 30 min of contact. In contrast, nanocolumnar cupric oxide (NC-CuO) thin films with a similar nanostructure exhibited weak activity [15]. This difference in the magnitude of inactivation can be attributed to the higher chemical stability of CuO compared with that of Cu [16,17]. However, it is not appropriate to conclude solely from this result that the nanostructure-imparted mechanical activity is weaker than the Cu-imparted chemical activity. This is because the method employed in prior research [15] was limited to wet conditions wherein the virus was encapsulated in a sufficient amount of solution, which reflects only a subset of actual conditions in which a virus remains infectious.

Human-generated droplets, ranging from large droplets measuring

* Corresponding author.
E-mail address: kei-shigetoh@mosk.tytlabs.co.jp (K. Shigetoh).

https://doi.org/10.1016/j.mtbio.2025.101803
Received 23 January 2025; Received in revised form 5 April 2025; Accepted 24 April 2025
Available online 24 April 2025

several hundred micrometers to aerosols with <5 μm in diameter, facilitate the transmission of viruses [7,18]. The influence of the size of aerosols and droplets, temperature, relative humidity, and the chemical composition of droplets on virus activity is discussed [19]. Aerosols or small-volume (picoliters) sessile droplets rapidly (within a few seconds) dry out on the surface [20]. Strategies to combat viruses under these two conditions—large droplets (wet conditions) and aerosols (dry conditions)—should considerably differ in mechanism. However, guidelines on the design of antiviral coatings do not account for this variation. A possible reason is the lack of methods for an accurate evaluation of viral activity under the two extreme conditions.

The methods used to evaluate viral activity under wet conditions, such as the plaque assay (using large viral droplets of several tens of microliter) [12,14,15], are unsuitable under dry conditions because of the unstable recovery of applied viruses adhered to specimens with a rough surface. A change in the shape of the virus observed *via* electron microscopy, such as TEM, is often considered an indicator of virus inactivation [12,21]; however, it is difficult to conduct conventional TEM observations of specimens in liquids. Moreover, potential damage to the virus due to chemical treatment before observation and electron beam irradiation during observation cannot be discounted [22]. Atomic force microscopy (AFM) enables the observation of the 3D shape of viruses in both liquid and in atmospheric conditions [23–25], which mimic the viral conditions of large droplets (wet conditions) and aerosols (dry conditions), respectively. Accordingly, in this study, we investigated the topographical properties of viruses without viral pretreatment under both wet and dry conditions using high-speed atomic force microscopy (HS-AFM) [26,27] and elucidated the antiviral mechanism (chemical and mechanical) of NC-Cu films under the two extreme conditions. Our findings indicate that the nanostructure-induced mechanical activity of antiviral coatings is driven by drying and is significant under practical conditions, providing novel insights into their chemical and mechanical activities.

2. Methods

2.1. Thin film fabrication and characterization

Thin films of Cu and its oxides were fabricated *via* the radio frequency sputtering method with a pure Cu target, in accordance with the procedure reported in a previous study [15]. The Cu and CuO thin films were deposited in 5-Pa Ar (purity 99.9999 %) and 5-Pa O_2 10 %–Ar 90 % atmosphere, respectively. The amount of material deposited during the process was monitored using a quartz crystal oscillator placed near the sample stage, and the amounts of materials deposited were regulated using a mechanical shutter. Polypropylene (PP) sheets (thickness: 0.2 mm) were used as substrates. The crystal phases of the fabricated films were characterized *via* X-ray diffraction (Ultima IV (Rigaku, Japan) with Cu Kα radiation) [15]. The nanostructures of the films were characterized using a field-emission scanning electron microscope (FE-SEM; S5500, HITACHI High-Tech, Japan) and a conventional atomic force microscope (AFM; Nanoscope V, Bruker, Japan) with cantilevers (SI-DF20, Hitachi High-Tech Corporation, Japan), and the results are shown in Fig. S1. The Cu and CuO thin films exhibited densely arranged columnar structures measuring 5–10 nm in width, which was in good agreement with that reported previously [15]. The thicknesses of the thin films were evaluated *via* a cross-sectional FE-SEM analysis after cleaving the deposited film with Si substrate that was set beside the sample. The film thickness was confirmed to be ~15 nm.

2.2. Preparation of viral solution

Similar to that in a previous study [15], the envelope-type bacteriophage φ6 (NBRC 105899) was used as the model virus. A lysogeny broth (LB) (Formedium) medium containing calcium chloride (2 mM) (Ca-added LB medium) was used to prepare stock suspensions. The bacteriophage φ6 was added to *Pseudomonas syringae* after incubated at 30 °C until its exponential growth phase. The prepared stock suspensions were purified using a size-exclusion chromatography column (EV Second L70, GL Sciences Inc., Japan). The retention of the infectivity of the purified viral solution was confirmed *via* the plaque assay method [15]. The viral titer was estimated using plaque-forming units (PFU). A typical viral titer was $\sim 1 \times 10^{11}$ PFU mL^{-1}.

2.3. HS-AFM measurements

Topographical investigation of the bacteriophages was conducted using an HS-AFM (SS-NEX, Research Institute of Biomolecule Metrology Co., Ltd., Japan). Cantilevers USC-f1.2-k0.15 (Nanoworld Corporation, Switzerland) (median radius <10 nm, half-cone angle 8°) and OMCL-AC200TS-C3 (Olympus Corporation, Japan) (radius 7 nm, half-cone angle <9°) were used for observations in solution and under atmosphere, respectively. Typical observation areas were 1–2 μm square; the resolution was 400 × 400 pixels; the frame rate was in the range of 6–12 s.

2.3.1. Observation procedure under wet conditions

The samples (PP substrates, NC-CuO, and NC-Cu films) were cut into approximately 3 mm squares. We deposited 2 μL of the viral solution onto the samples, which were then placed in a sealed container with a moistened absorbent cotton to prevent dust adhesion and volatilization of the droplet. After a few minutes of physisorption of viruses, the sample surface was gently rinsed with 10 μL of Milli-Q water after a predetermined time (10 or 40 min). The virus remaining on the sample surface was then observed *via* HS-AFM in 1/500 nutrient broth (NB) (Becton Dickinson) solution (NB solution was diluted 500 times in Milli-Q water). The 1/500 NB has been used to dilute virus suspensions in plaque assays [15].

2.3.2. Observation procedure under dry conditions

The samples (PP substrates, NC-CuO, and NC-Cu films) were cut into squares of approximately 3 mm and deposited with 2 μL of the viral solution. The resulting samples were placed in a container for a few minutes for the physisorption of the viruses. The sample surface was then gently rinsed with 10 μL of Milli-Q water, and excess droplets were quickly blown off using a dust blower. The sample was dried for 30 min in an indoor atmosphere before HS-AFM observation under atmospheric conditions. To prevent the adhesion of dust on samples during the drying period, a sterile disposable Petri dish was placed over the sample, and a clean plate was positioned underneath to create a gap between the Petri dish and the base for natural ventilation.

2.4. Image processing and analysis

The obtained HS-AFM images were subjected to background and noise reduction using Eagle 2.5.8 (HS-AFM operation software) with the same settings employed for background and noise removal in all the images. Thereafter, the images were analyzed using ImageJ (Ver. 1.54f). The HS-AFM images displayed in the main text were obtained using the software Gwyddion [28].

2.4.1. Particle recognition and feature extraction

The shape of the particles believed to be virus particles in the obtained HS-AFM images was identified and evaluated as follows. The images were binarized by setting a threshold value for the height (brightness) of the image, and the evaluation region (ROI: regions of interest) was then determined using the plugin "Analyze Particles." For example, Fig. S3 shows the results for viruses observed on a PP substrate before and after particle recognition. During particle recognition, the plugin "Watershed" was used to separate nearby particles (e.g., the particles indicated by two arrows in Figure S3B). Figure S3A and S3B show the ROI overlaid on the original image before and after particle

recognition, respectively.

The lower limit of the threshold area set during particle recognition was marginally higher to avoid recognizing the protrusions on the thin film (observed with a diameter range of 20–40 nm), and particles with a smaller area were excluded. Specifically, the range of the projection area S of the recognized particles was set to 1900–90000 nm^2. The reference values for the set threshold were $S = 1963$ nm^2 for a perfect circle with diameter $D = 50$ nm and $S = 90000$ nm^2 when $D = 340$ nm. Coarse particles suspected of agglomeration were eliminated based on the volume values. Finally, the lower and upper thresholds of the particle size for evaluation were determined based on the volume of the particles as follows. The lower and upper thresholds for the particle volume in the wet condition experiment were set to 10000 and 250000 nm^3, respectively (see next section for volume calculations). The lower and upper thresholds for the particle volume in the dry condition experiment were set to 1000 and 110000 nm^3, respectively. These thresholds for the upper and lower volumes were determined as ~4 times and ~0.1 times the median particle volume observed, respectively, on the PP substrate under wet and dry conditions. This is based on the fact that the typical envelope virus diameter distribution (volume is proportional to the cube of the diameter) is approximately 1.6 and 0.6 times the median values [12,29,30]. As an indicator of irregularity, circularity ($4\pi \times S/l^2$) obtained from S and the perimeter l was evaluated. The circularity is 1 [$4\pi \times \pi r^2/(2\pi r)^2$] for a perfect circle whereas shapes, such as rectangles or irregular polygons, have lower values.

2.4.2. Particle volume calculation

The method for estimating the volume under the particle, *i.e.*, background, is explained in the vertical cross-sectional schematics shown in Fig. S4A–C. The height profile of the particle region measured by HS-AFM is shown in Fig. S4A (solid black line in one dimension for simplification). The blue cylinder region (Fig. S4B), which includes the area below the particle inside the ROI identified by image analysis, was considered the background volume (BGv). Specifically, BGv (blue cylinder) was calculated by multiplying the mean value of the height at the outer edge of the ROI and the projected area S of the particle. The particle volume V, represented by the upper part of the particle (red hemisphere in Fig. S4C), was obtained by subtracting BGv from the volume inside the ROI (sum of the brightness values in the ROI). This V was estimated to be lower than the volume of the true spherical particle (gray sphere in Fig. S4A). However, the AFM probe cannot penetrate the area that is in the shadow of the particle when the particle is viewed from the vertical direction (Fig. S4A). Considering this limitation, the volume V shown in red, which does not include the shaded volume, was adopted here as the volume of the particle. No correction was applied for the probe width, as it did not significantly impact the analysis.

3. Results and discussion

3.1. Topographical properties of bacteriophages on fabricated NC-Cu and NC-CuO films under wet conditions

NC-Cu and NC-CuO films were fabricated on polypropylene (PP) substrates via the sputtering method [15]. Films with thickness ~15 nm and densely arranged nanocolumnar structures were obtained (Fig. S1). Purified viral solutions of bacteriophage φ6, an envelope-type virus, were used for the HS-AFM observations. For wet conditions, the bacteriophage φ6 in a dispersion (viral solution) was allowed to contact the samples for a predetermined time and observed in the solution using HS-AFM. The images obtained were analyzed using ImageJ software (Ver. 1.54f) [31] to determine the particles that appeared to be bacteriophages, and the volumes were compared. The nanocolumnar structures of the fabricated thin film and virus particles were distinguished by setting a height threshold and binarizing the images and then excluding the particles.

Fig. 1A shows an HS-AFM image of the particles observed in the solution after 40 min of exposure to the PP substrate. Round and spherical viruses were scattered over the PP substrate. The particle volume distribution (inset, Fig. 1A) shows peaks at ~150×10^3 nm^3 and ~40×10^3 nm^3. The particle volume distribution is not obviously different from that observed after a 10 min exposure (Fig. S2). Thus, the change in the volume of the virus particles over time in this time range is minimal. A magnified HS-AFM image and the corresponding line profiles of representative virus particles are shown in Fig. 1B and C, respectively. Virus particles measuring ~100 nm in diameter and ~60 nm in height were observed on PP. This bacteriophage φ6 particle size was comparable with that of reported values [15,29]. The virus particles on the NC-CuO surface were also round and scattered on the substrate (Fig. 1D). The volume distribution of the virus particles on NC-CuO (inset, Fig. 1D) was similar to that on PP, with two peaks centered at ~150×10^3 nm^3 and ~40×10^3 nm^3. Magnified view and line profiles (Fig. 1E and F) of the virus particles indicated a diameter of ~100 nm and height of ~60 nm, similar to those on PP. In contrast, the virus particles after 40 min of contact with the NC-Cu films were round but small in height (Fig. 1G); small particles measuring ~60 nm in diameter and ~30 nm in height were observed (Fig. 1H and I). A few particles in Fig. 1G that appear extremely bright were considered aggregates of vertically stacked viruses. These particles were excluded from analysis based on the upper particle-volume threshold described in the Methods section. The proportion of small-volume virus particles was higher than those in the cases of PP and NC-CuO films (insets of Fig. 1A, D, and 1G). The proportion of small particles increased with time to a value even greater than that observed when exposed to NC-Cu for 10 min (Fig. S2). High-resolution images were acquired to perform a more detailed characterization of the particles, particularly to compare the surface structure of the virus particles. Numerous indentations were observed (Fig. 1J) on the surface of the virus particles with a larger diameter (~100 nm) after 10 min of exposure to NC-Cu. These indentations were not observed in the cases of PP and NC-CuO, even for 40 min of exposure (Fig. 1K and L).

When considered in conjunction with the changing volume distribution of the virus on NC-Cu, the crack-like depressions appear to indicate the initial stages of destruction of the particles. The small particles observed on NC-Cu could correspond to the wreckage of damaged or disrupted virus particles, such as fragmented or reorganized lipid membranes [32–34] resulting from further damage. Dissolved Cu ions and generated ROS damage the cell membrane [35], viral envelopes, and proteins [13,14,36–39]. The disruption of the viral envelope after 30 min of exposure to copper plate has been observed *via* TEM [21]. The damage and disruption of cell membranes and model lipid bilayers by Cu ions leached from Cu nanoparticles have been investigated *via* trypan blue staining, and this effect has rarely been observed with CuO nanoparticles [40]. Accordingly, the chemically stable NC-CuO is believed to have inhibited the dissolution of Cu ions [16,17] and consequently, no apparent changes to the virus particle shape were observed. Moreover, the changes in the shape and volume of the virus particles observed herein are consistent with the results of our previous study (NC-Cu film ≫ NC-CuO film and PP), wherein the viral activity was evaluated *via* plaque assay under the same wet conditions as in this study [15]. Therefore, the change in the shape of the virus particles observed *via* HS-AFM can be reasonably considered as an indicator of antiviral activity. In this analysis, particles with volumes below ~40×10^3 nm^3 were regarded as virus particles that had sustained damage. In contrast, larger particles, with a volume distribution centered at ~150×10^3 nm^3, were considered representative of intact virus particles. No correction for the AFM probe width was applied in estimating particle volumes in this study. The overestimation of particle width caused by the probe geometry becomes increasingly significant for smaller particles [41,42]. Thus, applying such a correction [41] would likely accentuate the observed size difference between the two peaks in the particle volume distribution, corresponding to damaged and intact virus particles. Non-spherical particles, as observed by the mechanical activity of

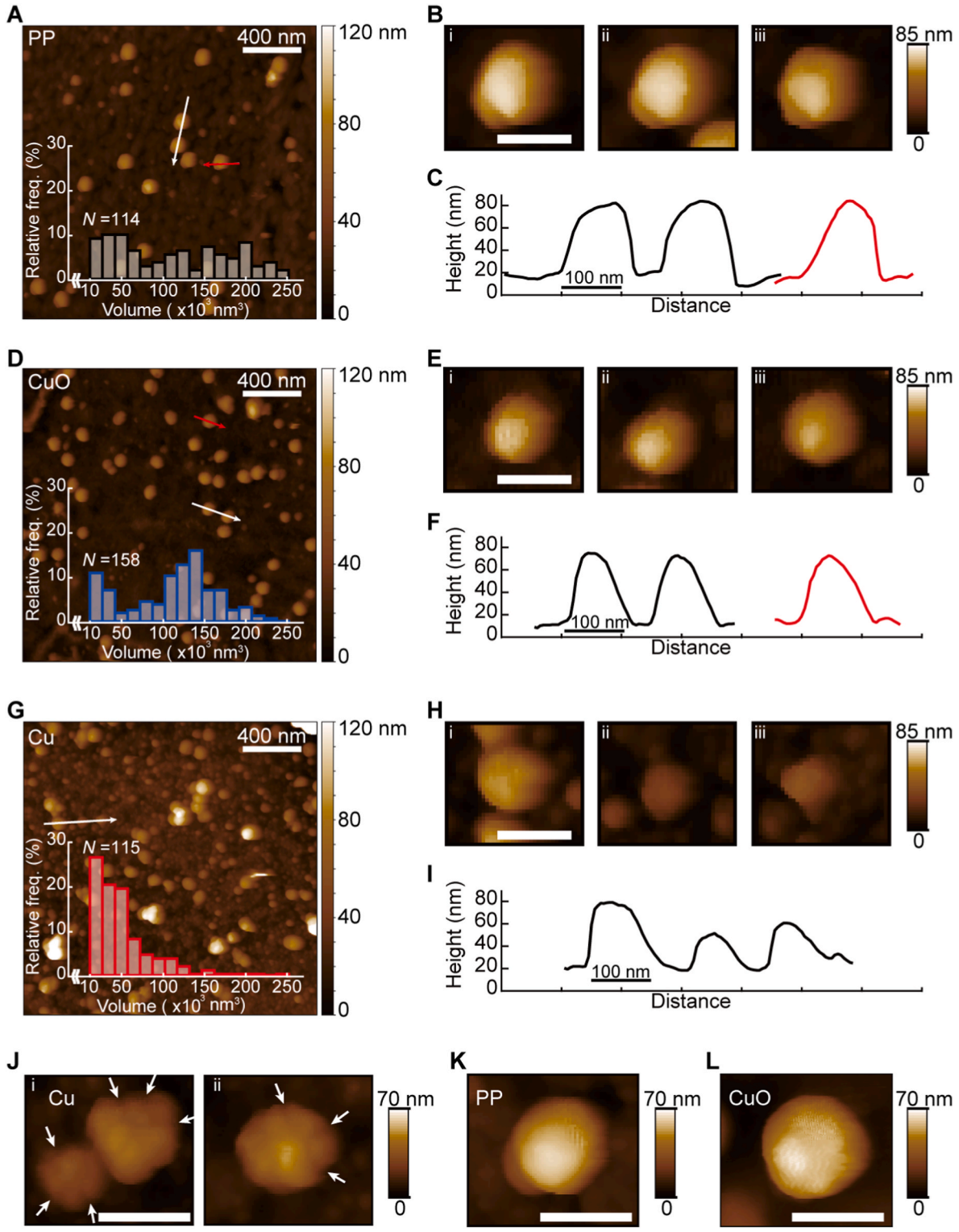

Fig. 1. Topographic structures of bacteriophage φ6 under wet conditions. (**A**) A typical HS-AFM image of the viruses observed in the solution after 40 min of contact with a PP surface under wet conditions. The inset is a histogram of the distribution of virus particle volume. (**B**) Magnified view of representative virus particles indicated by white and red arrows in (A). (**C**) Line profiles of particles indicated by white and red arrows in (A) shown as black and red lines, respectively. (**D**) A typical HS-AFM image of the viruses observed in the solution after 40 min of contact with an NC-CuO film surface under wet conditions. The inset is a histogram of the volume distribution of the virus particle. (**E**) Magnified view of representative virus particles indicated by white and red arrows in (D). (**F**) Line profiles of particles indicated by white and red arrows in (D) shown as black and red lines, respectively. (**G**) A typical HS-AFM image of the virus observed in the solution after 40 min of contact with an NC-Cu film surface under wet conditions. The inset is a histogram of the volume distribution of the virus particle. (**H**) Magnified view of representative virus particles indicated by a white arrow in (G). (**I**) Line profile of the particles indicated by white arrows in (G). (**J-L**) Magnified high-resolution HS-AFM images of the virus on each sample: (J) NC-Cu film after 10 min of exposure. The dented regions on the viral surface are indicated by arrows; (**K**) PP; and (**L**) NC-CuO film after 40 min of exposure. The scale bars (without values) are 100 nm.

nanospike silicon [12], were not observed, suggesting that the chemical antiviral activity of Cu is dominant under wet conditions.

3.2. Topographical properties of bacteriophages on fabricated NC-Cu and NC-CuO films under dry conditions

The viral solution was dropped on the sample, excess droplet was quickly blown off, and the sample was dried for 30 min under atmospheric conditions before HS-AFM observations. Fig. 2A shows an HS-AFM image of a bacteriophage φ6 particle on PP under dry conditions. Round and spherical viruses were scattered over the substrate. The particle volumes were normally distributed (inset, Fig. 2A) over the range of 10–60 × 10^3 nm^3 with a peak centered at ~30 × 10^3 nm^3. The diameter and height of a typical virus particle were ~90 nm and ~25 nm, respectively (Fig. 2B). The height of the virus particles on PP was lower (~2.4 times) than that under wet conditions (Fig. 1B and C). This shrinkage was likely due to drying because AFM observations have indicated that enveloped viruses (vaccinia virus) reversibly shrink in height by up to 2.5 times upon drying [23]. Because of the drying-induced shrinkage, a comparison of the shape changes of the particles based solely on their volume change under dry conditions may not be adequate. Therefore, we employed circularity, which can be calculated from the projected area and perimeter of particles, as a complementary indicator to evaluate the shape irregularities independent of volume. Particles on PP (Fig. 2C) were circular, and the circularity was generally high, with values around 0.9. The height of the particles on NC-CuO was lower than that of the particles on PP (Fig. 2D). The histograms in Fig. 2D show the particle volume distribution: the proportion of small particles on the NC-CuO surface was higher than that on the PP surface. The diameter and height of the particles on the NC-CuO film (inset, Fig. 2E), as revealed by the line profiles, were ~90 nm and ~10 nm, respectively; thus, these particles were flatter than those on the PP surface. The flat and non-spherical shape of the particles is evident from the 3D view of a representative particle shown in Fig. 2F. The relative frequency of circularity (~0.9) was lower than that on PP, and particles with a lower circularity of 0.7 were also observed. The particles on NC-Cu were smaller in height than those on PP (Fig. 2G). The proportion of small particles on NC-Cu was higher than that on PP (inset of Fig. 2G). The diameter and height of the particles on NC-Cu were ~90 nm and ~15 nm, respectively (inset of Fig. 2H); thus,

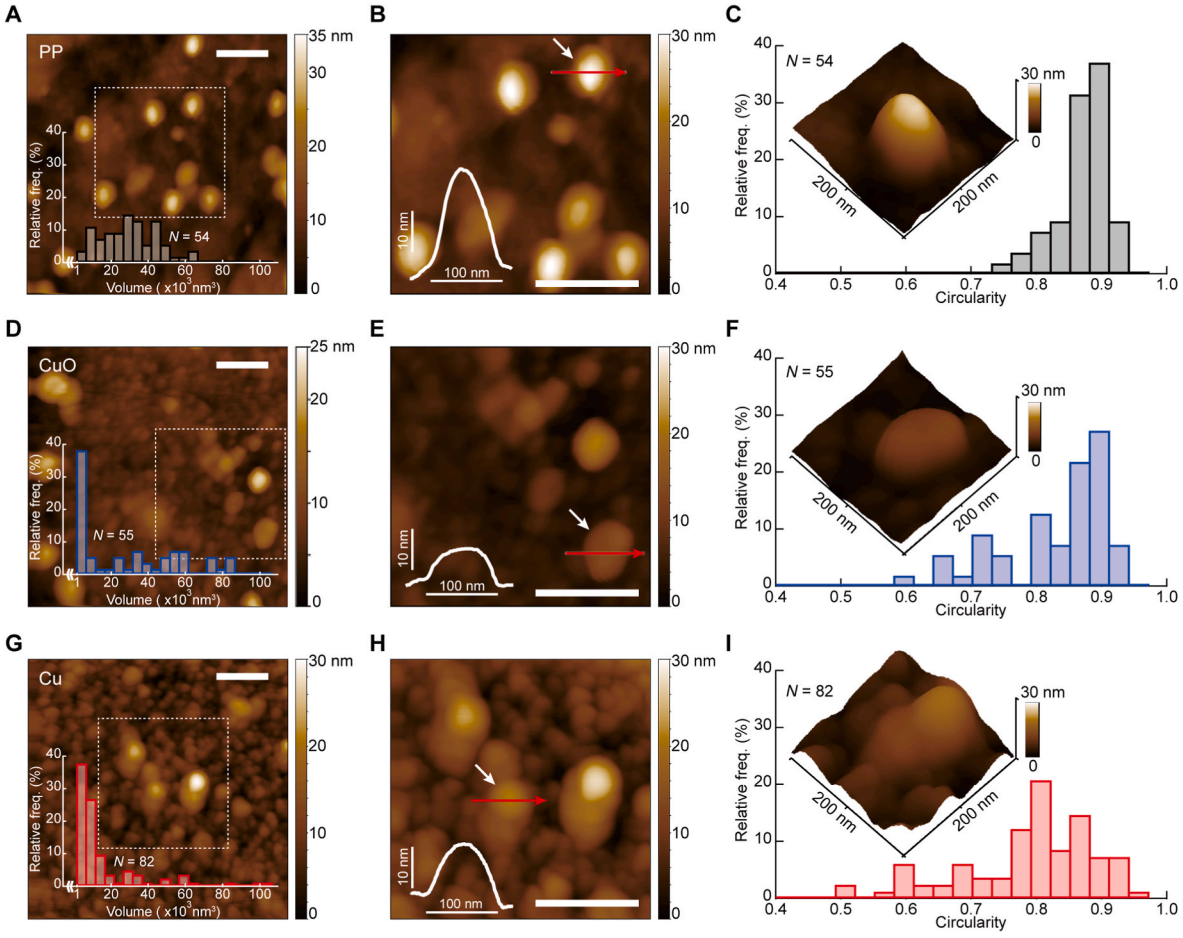

Fig. 2. Topographic structures of bacteriophage φ6 under dry conditions. **(A)** A typical HS-AFM image obtained under atmospheric conditions after exposing the virus to a PP surface for 30 min. The inset is a histogram of the volume distribution of the virus particles. **(B)** Magnified view of the area marked by a white dashed square in (A). The inset is a line profile along the direction indicated by the red arrow. **(C)** Circularity distribution of the virus particles on a PP surface under dry conditions. A 3D image of a representative particle indicated by a white arrow in (B) is shown in the inset. **(D)** A typical HS-AFM image obtained under atmospheric conditions after exposing the viruses to the NC-CuO film surface for 30 min under dry conditions. The inset is a histogram of the volume distribution of the virus particle. **(E)** Magnified view of the area marked by a white dashed square in (D). The inset shows a line profile along the direction indicated by the red arrow. **(F)** Circularity distribution of the virus particles observed on the NC-CuO surface under dry conditions. A 3D image of a representative particle indicated by a white arrow in (E) is shown in the inset. **(G)** A typical HS-AFM image obtained under atmospheric conditions after exposing the virus to the NC-Cu film surface under dry conditions for 30 min. The inset is a histogram of the volume distribution of the virus particle. **(H)** A magnified image of the area marked by a white dashed square in (G). The inset shows a line profile along the direction indicated by the red arrow. **(I)** Circularity distribution of the virus particles observed on the NC-Cu surface under dry conditions. A 3D image of a representative particle indicated by a white arrow in (H) is shown in the inset. The scale bars without values are 200 nm.

similar to the particles on NC-CuO, the particles on NC-Cu were flatter than those on PP. Fig. 2I shows a 3D view of a representative particle on NC-Cu: the non-spherical particle shape is evident. The most frequent distributions of circularity were shifted from ~0.9 (in the case of PP) to ~0.8. Notably, such a non-spherical (irregular) shape of the particles on the NC-CuO and NC-Cu films has been previously observed in the case of virus particles on the surface of nanospike silicon [12].

The fact that the NC-CuO film did not lead to an apparent change in the shape of the virus particles under wet conditions (Fig. 1) but caused a shape change and a volume reduction under dry conditions offers crucial insights (Fig. 2). Under dry conditions, both the leaching and transfer of Cu ions is further inhibited by the chemically stable CuO [16,17], resulting in weak antiviral activity. Moreover, the inactivation rate of bacteriophage φ6 due to dissolved Cu ions plateaus when the solution is depleted [43]. Nevertheless, the change in the shape of the virus particles on the NC-CuO film under dry conditions suggests that such a change is due to a mechanism distinct from the chemical activity of Cu (*i.e.*, mechanical activity). These results indicate that dry conditions drive the mechanical activity of the NC-CuO and NC-Cu films. Moreover, a higher number of non-spherical particles were observed on NC-Cu than on NC-CuO (Fig. 2F and I). However, it remains unclear whether this result is due to the synergistic effect of the mechanical activity and catalytic (called contact killing) activity [14,16,37,38] of Cu, working independently of the Cu ion leaching.

The data in recent reports that help argue for the existence of mechanical activity against the virus [11,12] support our consideration that drying is the driving force of mechanical activity. Nanostructured aluminum [11] and nanospike silicon [12], which show mechanical activity, require 3–6 h to exhibit an apparent (inactivation of one order of magnitude) difference in the antiviral activity compared with flat control samples. We expected a correlation between this time (3–6 h) and the time required for drying the ~20 μL viral droplets on the samples. The supplementary data for nanospike silicon, which show the amount of volatilization of the droplets, are in excellent agreement with expectations, with nearly complete drying occurring within 6 h [12]. This suggests that the well-established plaque assay method applied under wet conditions is not technically suitable for an accurate evaluation of the mechanical activity. In particular, mechanical activity potentially leads to results within a much shorter period, *i.e.*, 30 min of drying, under atmospheric conditions and is thus remarkably faster than the previously reported time period of 3–6 h [11,12]. Thus, the results obtained herein indicate for the first time that mechanical activity is not negligible but can be significant under dry conditions, *i.e.*, small droplets and aerosols.

We now discuss the mechanism of the mechanical activity of the NC-Cu and NC-CuO films that causes the virus to lose its shape integrity. A simulation of the mechanical action of the nanospike silicon *via* the finite element method indicates that the force induced solely from the contact between the spikes and the virus envelope is insufficient to cause piercing and that some external force is necessary [12]. This external force could be the tension generated by the shrinkage of the viruses immobilized on the nanocolumns upon drying. Additionally, the multi-point contact between the nanocolumns and the virus due to the loss of buoyancy after drying might trigger the destruction of the virus. Lipid bilayer rupture due to densely adhered nanoparticles has been experimentally and theoretically verified [44]. Even the adsorption of chemically stable gold nanoparticles leads to membrane rupture [44]. In our study, Cu and CuO were formed as thin films rather than nanoparticles but were densely arranged as columnar structures with a 10 nm diameter (pseudo-nanoparticles). Hence, NC-Cu with dense nanostructures could produce the same result as the gold nanoparticles.

3.3. Proposed primary mechanism of the antiviral activity of NC-Cu films under the wet and dry conditions

Based on the topographical properties of the virus under the wet and dry conditions described above, we propose a primary mechanism of the antiviral activity as follows. A schematic of the mechanism is shown in Fig. 3. Under wet conditions (Fig. 3A), when the virus is dispersed in a sufficient amount of solution, such as human saliva, buoyancy may lead to minimal contact between the virus and nanocolumns. Therefore, instead of the occasional direct contact between the viruses and nanocolumns, well-known chemical activities of Cu, such as eluted Cu ions and generated ROS, may inactivate suspended viruses through the solution [13,14,35–39]. In contrast, under dry conditions, the lack of a solution prevents not only the elution of Cu ions from the materials but also the transport of such reactive chemical agents to the target virus [43]. The number of contact points between the virus and nanocolumns increases because of the settling of the virus after solution evaporation. After further drying, the tension induced by the shrinkage of the virus pinned on the nanocolumns induces a significant force against the outer surface of the virus, resulting in mechanical destruction (Fig. 3B). This inactivation mechanism hypothesis suggests that the addition of nanostructures to chemically active materials (not limited to Cu) can help in seamless and efficient virus inactivation under dry, wet, and intermediate conditions.

4. Conclusion

In summary, we investigated the topographical properties of bacteriophage φ6 as an indicator of viral integrity using HS-AFM after exposure to NC-Cu and NC-CuO film surfaces under wet and dry conditions. These conditions represent the two extremes of the drying scenario after the adhesion of viral solutions owing to the significant (~nine orders of magnitude) volume differences between large droplets and aerosols constituting human-generated droplets. Under wet conditions, a reduction in the volume of the virus particles was observed within 40 min of exposure only for the NC-Cu film and not for the chemically stable NC-CuO film and PP. The difference in the shape change is consistent with the tendency of inactivation activity previously examined *via* plaque assay (wet conditions) [15]. Therefore, the reduction in the virus volume is primarily attributed to the chemical activity of Cu damaging and disrupting the virus envelope. Under dry conditions, non-spherical virus particles were observed on both the NC-CuO and NC-Cu films after merely 30 min of drying under atmospheric conditions. These non-spherical shapes were similar to those observed on nanospike silicon, which is considered to exhibit mechanical activity [12]. Thus, our NC-Cu film exhibits mechano-chemo-virucidal activity: it inactivates viruses through two independent mechanisms—chemical and mechanical activity under wet and dry conditions, respectively. The film exhibited potential mechanical activity against the virus in a considerably shorter time (30 min) under dry conditions compared with previously reported time periods (3–6 h). Thus, we demonstrate for the first time that inactivation *via* mechanical activity is driven by dry conditions and is not negligible but can be significant, especially for viruses in small droplets or aerosols. Methods to evaluate the infectious activity of viruses under dry conditions must be established in the future to clarify the detailed mechanism of mechanical activity and optimize the geometries of nanostructures. A steady and effective way to clarify the mechanical activity and optimize the geometry of nanostructures would be to compare nanostructured surfaces composed only of inert materials such as polymers. The results obtained herein provide novel insights into the roles of chemical and mechanical activities of antiviral coatings in practical environments and suggest new design guidelines.

CRediT authorship contribution statement

Keisuke Shigetoh: Writing – review & editing, Writing – original draft, Visualization, Validation, Supervision, Methodology, Investigation, Formal analysis, Data curation, Conceptualization. **Yusuke Hirata:** Writing – review & editing, Software, Methodology. **Nobuhiko**

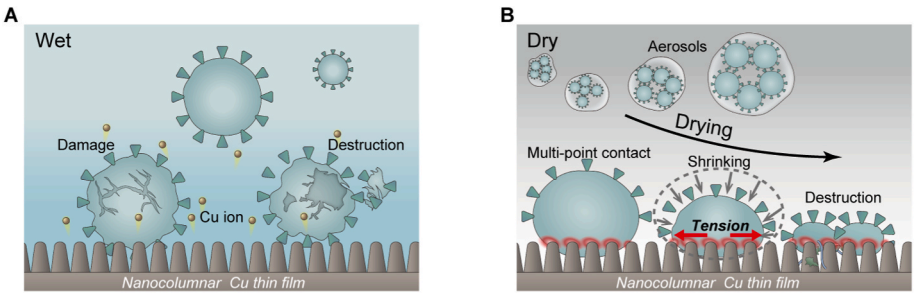

Fig. 3. Schematic of the primary virus inactivation mechanism by a nanocolumnar copper thin film. **(A)** Virus inactivation under wet conditions (virus in large droplets). Copper ions eluted from the thin film attack the virus, damaging and destroying its envelope and protein. **(B)** Virus inactivation under dry conditions (virus in aerosols). As the liquid containing the virus dries after adhering to the film, the virus comes into multi-point contact with the nanocolumns. The tension generated due to the virus pinning on the columns leads to the destruction of the virus.

Muramoto: Writing – review & editing, Supervision, Resources. **Nobuhiro Ishida:** Writing – review & editing, Supervision, Resources.

Declaration of competing interest

The authors declare that they have no known competing financial interests or personal relationships that could have appeared to influence the work reported in this paper.

Acknowledgements

The authors thank Dr. Norito Kotani and Mr. Ryo Nakatsuka from Research Institute of Biomolecule Metrology Co., Ltd. for their assistance in operating the HS-AFM equipment. We thank Ms. Rie Hirao for the support in the preparation of viral suspension and Mr. Keisuke Asano for helpful discussion on image analysis.

Appendix A. Supplementary data

Supplementary data to this article can be found online at https://doi.org/10.1016/j.mtbio.2025.101803.

Data availability

Data will be made available on request.

References

[1] E. Dong, H. Du, L. Gardner, An interactive web-based dashboard to track covid-19 in real time, Lancet Infect. Dis. 20 (2020) 533.
[2] Covid-19 dashboard by the center for systems science and engineering at Johns Hopkins university. https://gisanddata.maps.arcgis.com/apps/dashboards/bda7594740fd40299423467b48e9ecf6. (Accessed 8 November 2024).
[3] A.P. Mouritz, J. Galos, D.P. Linklater, R.B. Ladani, E. Kandare, R.J. Crawford, E. P. Ivanova, Towards antiviral polymer composites to combat Covid-19 transmission, Nano Sel 2 (2021) 2061.
[4] N. van Doremalen, T. Bushmaker, D.H. Morris, M.G. Holbrook, A. Gamble, B. N. Williamson, A. Tamin, J.L. Harcourt, N.J. Thornburg, S.I. Gerber, J.O. Lloyd-Smith, E. de Wit, V.J. Munster, Aerosol and surface stability of Sars-Cov-2 as compared with Sars-Cov-1, N. Engl. J. Med. 382 (2020) 1564.
[5] J. Sizun, M.W.N. Yu, P.J. Talbot, Survival of Human Coronaviruses 229e and Oc43 in Suspension and after Drying Onsurfaces: A Possible Source Ofhospital-Acquired Infections, J. Hosp. Infect. 46 (2000) 55.
[6] M.T. Brady, J. Evans, J. Cuartas, Survival and disinfection of parainfluenza viruses on environmental surfaces, Am. J. Infect. Control 18 (1990) 18.
[7] J. Joseph, H.M. Baby, S. Zhao, X.-L. Li, K.-C. Cheung, K. Swain, E. Agus, S. Ranganathan, J. Gao, J.N. Luo, N. Joshi, Role of bioaerosol in virus transmission and material-based countermeasures, Exploration 2 (2022) 20210038.
[8] S.M. Kelleher, O. Habimana, J. Lawler, B. O' Reilly, S. Daniels, E. Casey, A. Cowley, Cicada wing surface topography: an investigation into the bactericidal properties of nanostructural features, ACS Appl. Mater. Interfaces 8 (2016) 14966.
[9] A. Elbourne, R.J. Crawford, E.P. Ivanova, Nano-structured antimicrobial surfaces: from nature to synthetic analogues, J. Colloid Interface Sci. 508 (2017) 603.
[10] D.P. Linklater, V.A. Baulin, S. Juodkazis, R.J. Crawford, P. Stoodley, E.P. Ivanova, Mechano-bactericidal actions of nanostructured surfaces, Nat. Rev. Microbiol. 19 (2021) 8.
[11] J. Hasan, Y. Xu, T. Yarlagadda, M. Schuetz, K. Spann, P.K.D.V. Yarlagadda, Antiviral and antibacterial nanostructured surfaces with excellent mechanical properties for hospital applications, ACS Biomater. Sci. Eng. 6 (2020) 3608.
[12] S.W.L. Mah, D.P. Linklater, V. Tzanov, P.H. Le, C. Dekiwadia, E. Mayes, R. Simons, D.J. Eyckens, G. Moad, S. Saita, S. Joudkazis, D.A. Jans, V.A. Baulin, N.A. Borg, E. P. Ivanova, Piercing of the human parainfluenza virus by nanostructured surfaces, ACS Nano 18 (2024) 1404.
[13] M. Minoshima, Y. Lu, T. Kimura, R. Nakano, H. Ishiguro, Y. Kubota, K. Hashimoto, K. Sunada, Comparison of the antiviral effect of solid-state copper and silver compounds, J. Hazard Mater. 312 (2016) 1.
[14] K. Sunada, M. Minoshima, K. Hashimoto, Highly efficient antiviral and antibacterial activities of solid-state cuprous compounds, J. Hazard Mater. 235–236 (2012) 265.
[15] K. Shigetoh, R. Hirao, N. Ishida, Durability and surface oxidation states of antiviral nano-columnar copper thin films, ACS Appl. Mater. Interfaces 15 (2023) 20398.
[16] M. Hans, A. Erbe, S. Mathews, Y. Chen, M. Solioz, F. Mücklich, Role of copper oxides in contact killing of bacteria, Langmuir 29 (2013) 16160.
[17] Y. Rodhe, S. Skoglund, I. Odnevall Wallinder, Z. Potácová, L. Möller, Copper-based nanoparticles induce high toxicity in leukemic Hl60 cells, Toxicol. Vitro 29 (2015) 1711.
[18] C.C. Wang, K.A. Prather, J. Sznitman, J.L. Jimenez, S.S. Lakdawala, Z. Tufekci, L. C. Marr, Airborne transmission of respiratory viruses, Science 373 (6558) (2021) eabd9149.
[19] A.K. Longest, N.C. Rockey, S.S. Lakdawala, L.C. Marr, Review of factors affecting virus inactivation in aerosols and droplets, J. R. Soc. Interface 21 (2024) 20240018.
[20] E.L. Talbot, A. Berson, P.S. Brown, C.D. Bain, Evaporation of picoliter droplets on surfaces with a range of wettabilities and thermal conductivities, Phys. Rev. E 85 (2012) 061604.
[21] L. Warnes Sarah, R. Little Zoë, C.W. Keevil, Human Coronavirus 229e Remains Infectious on Common Touch Surface Materials, mBio 6 (2015).
[22] B.M. Zaki, A.A. Mohamed, A. Dawoud, K. Essam, Z.K. Hammouda, A. S. Abdelsattar, A. El-Shibiny, Chapter Two - Isolation, Screening and Characterization of Phage, vol. 200, Academic Press, 2023, p. 13.
[23] A.J. Malkin, A. McPherson, P.D. Gershon, Structure of intracellular mature vaccinia virus visualized by in situ atomic force microscopy, J. Virol. 77 (2003) 6332.
[24] E.V. Dubrovin, A.G. Voloshin, S.V. Kraevsky, T.E. Ignatyuk, S.S. Abramchuk, I. V. Yaminsky, S.G. Ignatov, Atomic force microscopy investigation of phage infection of bacteria, Langmuir 24 (2008) 13068.
[25] K. Lim, N. Kodera, H. Wang, M.S. Mohamed, M. Hazawa, A. Kobayashi, T. Yoshida, R. Hanayama, S. Yano, T. Ando, R.W. Wong, High-speed afm reveals molecular dynamics of human influenza a hemagglutinin and its interaction with exosomes, Nano Lett. 20 (2020) 6320.
[26] T. Ando, T. Uchihashi, T. Fukuma, High-speed atomic force microscopy for nano-visualization of dynamic biomolecular processes, Prog. Surf. Sci. 83 (2008) 337.
[27] N. Kodera, D. Yamamoto, R. Ishikawa, T. Ando, Video imaging of walking myosin V by high-speed atomic force microscopy, Nature 468 (2010) 72.
[28] Free spm data analysis software. http://gwyddion.net/. (Accessed 24 January 2024).
[29] Á. Serrano-Aroca, Antiviral characterization of advanced materials: use of bacteriophage phi 6 as Surrogate of enveloped viruses such as Sars-Cov-2, Int. J. Mol. Sci. 23 (2022).
[30] B. Kiss, Z. Kis, B. Pályi, M.S.Z. Kellermayer, Topography, spike Dynamics, and Nanomechanics of Individual native Sars-Cov-2 Virions, Nano Lett. 21 (2021) 2675.
[31] C.A. Schneider, W.S. Rasband, K.W. Eliceiri, Nih image to imagej: 25 Years of image analysis, Nat. Methods 9 (2012) 671.
[32] M. Antonietti, S. Förster, Vesicles and liposomes: a self-assembly principle beyond lipids, Adv. Mater. 15 (2003) 1323.
[33] C. Huang, D. Quinn, Y. Sadovsky, S. Suresh, K.J. Hsia, Formation and size distribution of self-assembled vesicles, Proc. Natl. Acad. Sci. 114 (2017) 2910.
[34] M.A. Iriarte-Alonso, A.M. Bittner, S. Chiantia, Influenza a virus hemagglutinin prevents extensive membrane damage upon dehydration, BBA Adv. 2 (2022) 100048.

[35] B.A. VanWinkle, K.L. De Mesy Bentley, J.M. Malecki, K.K. Gunter, I.M. Evans, A. Elder, J.N. Finkelstein, G. Oberdörster, T.E. Gunter, Nanoparticle (Np) uptake by type I alveolar epithelial cells and their oxidant stress response, Nanotoxicology 3 (2009) 307.
[36] N. Wang, A.R. Ferhan, B.K. Yoon, J.A. Jackman, N.-J. Cho, T. Majima, Chemical design principles of next-generation antiviral surface coatings, Chem. Soc. Rev. 50 (2021) 9741.
[37] X. Fan, L.H. Yahia, E. Sacher, Antimicrobial properties of the Ag, Cu nanoparticle system, Biology 10 (2021) 137.
[38] V. Govind, S. Bharadwaj, M.R. Sai Ganesh, J. Vishnu, K.V. Shankar, B. Shankar, R. Rajesh, Antiviral properties of copper and its alloys to inactivate covid-19 virus: a review, Biometals 34 (2021) 1217.
[39] J.L. Sagripanti, L.B. Routson, C.D. Lytle, Virus inactivation by copper or iron ions alone and in the presence of peroxide, Appl. Environ. Microbiol. 59 (1993) 4374.
[40] H.L. Karlsson, P. Cronholm, Y. Hedberg, M. Tornberg, L. De Battice, S. Svedhem, I. O. Wallinder, Cell membrane damage and protein interaction induced by copper containing nanoparticles—importance of the metal release process, Toxicology 313 (2013) 59.
[41] V. Garcia, L. Martinez, J. Briceno-Valero, C. Schilling, Dimensional Metrology of nanometric spherical particles using AFM, Probe Microsc. 1 (1997) 107.
[42] A. Yacoot, L. Koenders, Aspects of scanning force microscope probes and their effects on dimensional measurement, J. Phys. D Appl. Phys. 41 (2008) 103001.
[43] J. Li, J. Dennehy John, Differential bacteriophage mortality on exposure to copper, Appl. Environ. Microbiol. 77 (2011) 6878.
[44] D.P. Linklater, V.A. Baulin, X. Le Guével, J.-B. Fleury, E. Hanssen, T.H.P. Nguyen, S. Juodkazis, G. Bryant, R.J. Crawford, P. Stoodley, E.P. Ivanova, Antibacterial action of nanoparticles by lethal stretching of bacterial cell membranes, Adv. Mater. 32 (2020) 2005679.